BIOMEDIATION OF SEDIMENT GRAVITY FLOW DYNAMICS

Melissa J. Craig[1]*
Jaco H. Baas[2]
Kathryn J. Amos[1]
Lorna J. Strachan[3]
Andrew J. Manning[4,5]
David M. Paterson[6]
Julie A. Hope[7]
Scott D. Nodder[8]
Megan L. Baker[2]

[1] Australian School of Petroleum, The University of Adelaide, Adelaide, South Australia, Australia
[2] School of Ocean Sciences, Bangor University, Menai Bridge, Isle of Anglesey, LL59 5AB, UK
[3] School of Environment, University of Auckland, Private Bag 92019, Auckland, New Zealand
[4] School of Marine Science and Engineering, Plymouth University, Drake Circus, PL4 8AA, UK
[5] HR Wallingford, Howbery Park, Wallingford, OX10 8BA, UK
[6] Scottish Oceans Institute, School of Biology, University of St Andrews, St Andrews, KY16 8LB, UK
[7] Institute of Marine Science, University of Auckland, Private Bag 92019, Auckland, New Zealand
[8] National Institute of Water & Atmospheric Research (NIWA), Private Bag 14901, Kilbirnie, Wellington 6241, New Zealand

*Corresponding author: melissa.craig@adelaide.edu.au

Keywords: fine-grained sediment, sediment gravity flows, extracellular polymeric substances, biological cohesion, sediment dynamics

Sediment gravity flows (SGFs) are the primary process by which sediment and organic carbon are transported from the continental margin to the deep ocean. Forty percent of the total marine organic carbon pool is represented by cohesive extracellular polymeric substances (EPS) produced by marine benthic and pelagic micro-organisms. EPS research to date has focussed on coastal environments, where EPS contribute to seabed stability by forming a cohesive matrix of bonds between sediment particles. The effects of this cohesive material on SGFs in the deep ocean have not been investigated, despite many decades of outcrop, subsurface, modern real-time observational, numerical, and experimental research. Here we present laboratory data that offer the first insights into the potential of biological cohesion for modulating muddy, physically cohesive, SGF dynamics. These data indicate that turbulence-modulated, high-density turbidity currents, mudflows and slides, are more susceptible to changes in flow properties than fully turbulent, low-density turbidity currents at concentrations of EPS encountered in the deep ocean. Even relatively low concentrations of EPS markedly decrease the head velocity and run-out distance of these high-density SGFs. These outcomes greatly improve our understanding of the natural distribution of SGF deposits, which form the world's largest hydrocarbon reservoirs.

Mud, inherently associated with organic matter, is the most abundant sediment type on the Earth[1, 2], and many examples of mud-rich SGFs have been documented in modern[3, 4] and ancient[5, 6] marine and lacustrine environments. Over the last two decades, advances in our understanding of the properties of cohesive mud have redefined the interpretation of flow dynamics and deposits of SGFs. Consisting predominantly of silt- and clay-sized particles, mud-rich SGFs are significantly influenced by the ability of clay minerals to aggregate, or flocculate[5, 7]. Flocculation occurs when clay platelets are brought into contact with each other and the electrostatic attractive forces between particles overcome the repulsive forces[8, 9]. At sufficiently high concentrations of clay, flocs bind together to form a network of linked clay platelets that increases the viscosity of the clay-water suspension[10]. Laboratory experiments of SGFs that contain high concentrations of clay show that this network behaves as a gel, measurably suppressing the shear-induced turbulence generated within the SGFs, causing a transition towards a laminar flow regime, and producing deposits that are radically different from fully turbulent SGFs[10, 11].

EPS enhance the natural tendency of clay particles to flocculate by adding biological cohesion, thus altering the physical and chemical properties of the flocs and therefore their transport and deposition[12, 13, 14]. EPS also stabilise the seabed by forming biofilms, composed of a matrix of sediment, single-cell organisms, and EPS, which behave as a surficial layer, preventing sediment transport until a threshold velocity is reached and the biofilm fails, after which the biofilm-bound sediment is entrained into the flow[15]. Recent experiments conducted under estuarine conditions demonstrate that the current mathematical predictors of bedform dimensions, based on non-cohesive sediment, significantly underestimate the combined effect of physical and biological cohesion on reducing bedform dimensions[16]. Very small amounts of EPS (< 0.063% by weight), representing pervasive background content in estuarine mixed sand and mud deposits, can also increase the development time of bedforms by two orders of magnitude[17]. Here we illustrate that the ability of EPS to bind sediment particles extends into SGFs and its effect on flow dynamics is at least as significant as the effect of physically cohesive sediment. This has important implications for the understanding of flow dynamics and deposits of SGFs that contain organic matter, and the global carbon cycle.

Methods

The experimental SGFs were generated in a 5 m long, 0.2 m wide, and 0.5 m deep, smooth-bottomed lock-exchange tank (Supplementary Figure 1). The reservoir within the tank was filled with a mixture of kaolinite clay (median grain size D_{50} = 9.1 µm; volumetric concentration C_{vol} = 5% - 23%), EPS, and seawater (Table 1). Xanthan gum, a commercially available biopolymer, was used as a proxy for natural EPS[14, 18]. The range of EPS dry weight concentrations used in the experiments matched the range measured from seabed sediment cores obtained during RV *Tangaroa* cruise TAN1604 in 2016, from 127 to 1872 m water depth in and offshore from the Hauraki Gulf, New Zealand (Supplementary Figures 2, 3; Supplementary Table 1). To our knowledge, these are the first cores collected for EPS analysis in the deep marine environment. The EPS data from these cores are based on the bulk carbohydrate content, using the standard Dubois assay method[19]. The maximum concentration by weight recorded was 0.260% from CS19, the deepest core site, with an average across all cores of 0.139%. This range of measured EPS concentrations were the basis of those used in the experimental SGFs, i.e. 0 - 0.268% (Table 1).

We tested the hypothesis that the biological cohesion provided by EPS intensifies cohesive flow behaviour by comparing the head velocity (U_h) and the run-out distance of clay-only control flows with equivalent flows containing EPS. Head velocity versus horizontal distance was obtained for each SGF using a high-definition video camera that tracked the flow along the tank, calculating the distance travelled between video frames against a scale along the tank bottom (Figure 3). Flow run-out distances, defined as the distance from the lock gate to the frontal end of the deposit, were recorded, except for flows that reflected off the end of the tank (Table 1). The flows were also studied visually using the video footage to determine if the EPS induced a transition in flow behaviour from that in the clay-only controls.

Results

Flows without EPS. The clay-only control flows generated low-density turbidity currents[20] (LDTCs) at C_{vol} = 5% - 15% and high-density turbidity currents[20] (HDTCs) at C_{vol} = 22% - 23%, allowing us to examine the effect of EPS in fully turbulent flows and in transitional flows experiencing some turbulence suppression by physical cohesion, respectively[20, 21]. The LDTCs (F01, F04 and F07) travelled the full length of the tank and reflected off the end wall. These flows generated Kelvin-Helmholtz instabilities along the upper interface with the ambient fluid (Figure 1). The HDTCs (F11 and F16) featured a dense lower layer with coherent fluid entrainment structures[22] (Supplementary Figures 9, 11); this dense layer transitioned upwards into a dilute mixing layer (Figure 2). Both HDTCs recorded a run-out distance within the tank, with F11 travelling further and reaching a higher maximum head velocity ($U_{h,m}$) than F16 (Table 1).

Low-density flows with EPS. At C_{vol} < 15%, the addition of EPS produced no measurable difference in the U_h profiles compared to the clay-only control (Supplementary Figures 4, 5) and all these flows were classified as fully turbulent LDTCs. At C_{vol} = 15%, the EPS-laden flows (F08, F09 and F10) were also visually indistinguishable from the clay-only flow (F07), all appearing as LDTCs. Although adding EPS had no effect on $U_{h,m}$ (Table 1), it is apparent that the head velocity of runs F08 and F09 began to decrease more rapidly than that of F07 between 4 m and 4.2 m along the tank, resulting in lower U_h-values at 4.6 m (Figure 3). For run F10, which carried the highest concentration of EPS, rapid flow deceleration began at 2.5 m, and the run-out distance was 3.9 m.

High-density flows with EPS. The 22% and 23% clay flow data demonstrate distinct decreases in U_h and run-out distance as EPS were added to the flow (Table 1, Figure 3, Supplementary Figure 6). When normalized to their respective clay-only $U_{h,max}$ and run-out distance, the combined 22% and 23% data show strong correlations with the amount of EPS added to the flow (for $U_{h,max}$, R^2 =0.82, p=0.0003, n=10; for run-out distances, R^2 = 0.90, p=0.00003, n=10; Supplementary Figures 7, 8). The addition of EPS at concentrations ≤ 0.089% to 22% clay still produced HDTCs, but these flows had a lower $U_{h,m}$ and a shorter run-out distance than the clay-only HDTCs (Supplementary Figure 6). EPS concentrations ≥ 0.133% in F14 and F15, however, dramatically reduced upper boundary mixing, thus producing a distinct interface with the ambient fluid, characteristic of cohesive debris flows (Supplementary Figure 10)[11, 23]. Flows F14 and F15 also lacked coherent fluid entrainment structures. On the basis of available fine sediment size, these flows have been classified as cohesive mudflow[20]. These highly cohesive mudflows could only achieve a $U_{h,m}$ less than half of that of the 22% clay-only and clay-EPS HDTCs, and 'en-masse' settling significantly reduced the run-out distance (Supplementary Figure 6). At C_{vol} = 23%, this change from HDTC to cohesive mudflow occurred at EPS concentrations ≥ 0.087%, showing a strong inverse relationship between EPS concentration and U_h and run-out distance (Figure 3). At the highest EPS concentration of 0.259% in F20, the slurry was incapable of establishing a well-defined flow and slid out of the lock-exchange reservoir for a short distance only (0.6 m). F20 thus resembled the coherent translation of sediment as a submarine slide[24].

Discussion

Effect of EPS on flow properties. Our experimental data demonstrate that the strong biological cohesion imparted by EPS within the seabed[16, 17] extends to SGFs. SGF head velocity and run-out distance are reduced following the addition of EPS to the HDTCs and the densest LDTCs. This effect was amplified with increasing suspended sediment concentration. At higher concentrations of clay and EPS, the biological cohesion caused a shift in flow type from HDTC to cohesive mudflow and slide. This suggests that the EPS were capable of attenuating shear turbulence and thus increasing the resistance and sustaining the bonds between clay particles in these SGFs[17]. This EPS-induced cohesion was greater, per unit weight, than the physical cohesion imparted by the clay. At 22% clay, the addition of a mere 0.133% EPS induced a flow transition from HDTC (F11) to cohesive mudflow (F14), whilst substantially reducing the run-out distance and $U_{h,m}$. A similar reduction in run-out

distance requires an increase in clay concentration from 22% to 25% in an EPS-free flow[22]. Adding 0.259% EPS to the 23% clay flow reduced the run-out distance by *c.* 3 m; 29% clay is needed in an equivalent EPS-free flow to attain a similar reduction[22].

Building upon earlier literature[12], Malarkey *et al.*[17] attributed the strong cohesion imparted by EPS within bedforms of cohesive sand to the ability of EPS to form thin filaments that bridge grains and inhibit these grains from moving independently, hence requiring smaller volumes of EPS, compared to clay, to reach similar bed strength. Similarly during transport, EPS in biofilm-coated sand grains act as a 'bio-glue,' binding clay particles and diatoms to the sand grains, which can remain as aggregates as far as 27 km from the nearest river mouth[25]. In aqueous sediment suspensions, EPS strengthen flocs and may assist in building a network of interconnected flocs, *i.e.* a gel, with a pseudo-plastic rheology at sufficiently high sediment concentrations[12]. We hypothesise that this process extends to SGFs. EPS in HDTCs are brought into contact with a greater number of clay particles than in LDTCs, allowing the EPS to integrate into the particle network and strengthen it, further suppressing turbulence, and encouraging a laminar regime within the sediment flow.

Gel strength. To test this hypothesis, the LabSFLOC-2 method (see Supplementary Methods) was used to compare samples of fluid taken directly from clay-only HDTC F16 and clay-EPS HDTC F17 for the analysis of floc size, settling velocity, and floc density. Figure 4 depicts floc populations extracted from the dense, gelled, lower layer of the flow head of both HDTCs at 60% of their run-out distance. As each sample was released into the LabsSFLOC-2 settling column, the gel underwent gravitational settling and broke up into flocs. Only 10% of the flocs in the clay-only flow were larger than 200 μm, compared to 55% of the flocs in the clay-EPS flow (Figure 4). Moreover, the difference in the density of the flocs increased as the floc size increased, with the clay-EPS flocs showing a lower density than the clay-only flocs by one order of magnitude at the highest settling velocity (Figure 4). This dominance of large, water-rich flocs in the clay-EPS flow implies that the clay-EPS gel was more cohesive than the clay-only gel, preventing the clay-EPS gel from breaking into smaller flocs under shear during static settling. In turn, we infer that the clay-EPS HDTC was more resistant to shear turbulence than the clay-only HDTC, and that this difference increased with increasing clay and EPS concentration, eventually resulting in less mobile, laminar mudflows and slides.

EPS in natural SGFs. The influence of EPS on the dynamics of the experimental SGFs was observed to extend across turbulent, transitional, and laminar flow types with complex and variable rheological properties. This renders the scaling of these flows to natural prototypes a non-trivial task, and standard methods, such as dimensionless Froude and Reynolds number, Shields parameter, and distorted geometric scaling, are unlikely to be valid without modification[21, 23, 26, 27]. However, the experimental SGFs may be used as an analogue for natural SGFs based on fundamental physical principles. The most suitable analogues are the 'weak' natural SGFs of Talling et al.[28] with velocities up to *c.* 0.5 ms^{-1}, and natural SGFs that have decelerated to a velocity similar to that of the experimental flows. 'Strong' and 'very strong' natural SGFs[28], on the other hand, reach speeds of up to several tens of metres per second. Such flows produce stronger shear turbulence than the experimental SGFs, and the development of natural HDTCs, cohesive mudflows, and slides therefore requires higher clay concentrations. However, adding EPS to all natural SGFs in which the clay attenuates the turbulence should contribute to a reduction in head velocity and run-out distance in ways similar to the experimental flows, because Baker *et al.*[22] showed that a small increase in the yield strength of turbulence-attenuated flows – here assumed to be driven by strongly cohesive EPS – has a large effect on flow behaviour, independent of flow velocity. Moreover, it is likely that turbulence attenuation is promoted further by the fact that flow viscosity and yield strength increase exponentially as flow density increases[29], and that in these denser flows the EPS concentration is higher, because less ambient water is added during seabed failure, erosion, and subsequent flow generation.

Implications for geology and engineering. Our study suggests that small but prevalent levels of EPS, as in the cores from the Hauraki Gulf, are sufficient to change turbulent SGFs into partly or fully laminar SGFs in the deep ocean. This could have a significant impact on the frequency of occurrence of turbulence-attenuated flows and their deposits. Hybrid event beds[7, 30], formed by a combination of turbulent turbidity currents and laminar debris flows, and the deposits of slurry flows and other types of cohesive SGFs[31, 32], have proved to be more common in the geological record than previously thought. The presence of biological cohesion in the high-density SGFs that formed these deposits helps to explain their common occurrence. The deposits formed by LDTCs, HDTCs, mudflows, and slides are distinctly different from each other owing to differences in the mechanisms of sediment deposition; EPS appear to promote the generation of shorter run-outs and therefore thicker deposits. The recognition that EPS promote slower and shorter-distance transport of sediment by HDTCs,

cohesive mudflows, and slides has economic implications, because SGFs damage infrastructure, such as communication cables on the seafloor[22], and contribute to the formation of organic matter-rich, deep-marine sedimentary sequences. These sequences are the source of hydrocarbons that can be stored in deposits of sandy SGFs[33] which form the world's largest hydrocarbon reservoirs[34].

Implications for the global carbon cycle. The burial of organic carbon in marine sediments represents the second largest sink of atmospheric CO_2[35] and is a major control on climate over geological timescales[36, 37]. Many sedimentary and biogeochemical factors affect the distribution, burial, and preservation efficiencies of organic carbon in oceanic sediments, in addition to those controlling the input and local primary production of organic material[37, 38]. More than 40% of organic carbon burial in the ocean occurs on the continental margin[39], where the continental slope forms a major sink of organic carbon[40, 41], with generally unfavourable preservation conditions on the continental shelf[38]. At water depths < 2000 m, clays show a strong correlation with the presence of organic material[38, 40]. The interaction between the organic matter and the clay has been proposed as the reason for this high concentration of organic matter on the continental slope[40]. Research has discussed various protection mechanisms provided by clays and other fine-grained sediments[38] to account for the elevated levels of organic carbon, but little attention has been given to the processes controlling the distribution of these organic-rich fine-grained deposits on the continental slope. Sedimentary processes, particularly SGFs, play a major role in the transportation of organic material and the eventual location of deposition[41]. Our results provide a possible process interpretation for the concentrated distribution of organic material onto the continental slope.

EPS shorten the run-out distance of high-density SGFs, such as HDTCs and cohesive mudflows, suggesting that clay-rich SGFs that are initiated on the shelf are encouraged by EPS to deposit more proximally on the continental slope than equivalent flows without EPS. This is supported by the observation that less mobile, cohesive debris flows of moderate to high strength tend to deposit mainly on the continental slope, and the deposits of more mobile debris flows of low strength dominate the deeper ocean[32]. The positive correlation between CO_2 concentration and the production of exopolymers like EPS renders EPS a direct sink of atmospheric CO_2 acquired by diatoms and other phytoplankton[42]. Therefore, by encouraging more proximal deposition of cohesive clay via dense SGFs, EPS contribute to the observed carbon sink in continental margin sediments.

Concluding Remarks

An increasing number of studies have highlighted the importance of considering physically cohesive material when interpreting and modelling SGF processes, but the insights into biologically cohesive SGFs presented herein indicate a need to recognise the potent effects of EPS in future studies. EPS are expected to be present in both modern and ancient SGFs and, at the levels encountered in both the modern estuarine and deep marine environments, EPS have proven capable of changing flow behaviour and reducing the deposit run-out lengths and maximum head velocity of cohesive flows. This research improves our understanding of the biological mediation of the mechanics of deep sea sediment transport. Further studies are needed to better constrain the effects of EPS on process models for both cohesive and non-cohesive SGFs, and the wider environmental relevance for deep sea engineering, geological history and the global carbon cycle.

Acknowledgements

We are very grateful to the Australian Government Research Training Program (RTP) Scholarship for funding M.J.C.'s PhD candidature and to the International Association of Sedimentologists for their Postgraduate Award Grant which funded M.J.C.'s visit to Bangor University to complete additional experiments imperative to this work. We would also like to acknowledge the U.K. Natural Environment Research Council for grant NE/1027223/1 (COHBED project) that enabled this research to be undertaken, using the flume facility kindly built by Bangor University technician Rob Evans. We also thank Brian Scannell, Edward Lock and Connor McCarron for their help in the laboratory. Irvine Davidson is thanked for his help in the measurement of EPS content in the Hauraki Gulf cores.

Author Contributions

J.H.B., K.J.A., L.J.S. conceived the study and all contributed significantly to writing the paper; M.J.C. carried out the experimental work and wrote the paper; A.J.M. collected and processed the LabSFLOC-2 data; D.M.P. and J.A.H. led the EPS content analysis of the Hauraki Gulf cores; S.D.N. collected the Hauraki Gulf cores; M.L.B. assisted in the laboratory work and contributed to writing.

Competing Financial Interests Statement

This study involves no competing financial interests.

References Cited

1. Hillier S. Erosion, sedimentation and sedimentary origin of clays. *Origin and Mineralogy of Clays*. Springer, 1995, pp 162-219.

2. Healy T, Wang Y, Healy J-A. *Muddy coasts of the world: processes, deposits and function*, vol. 4. Gulf Professional Publishing, 2002.

3. Bhattacharya JP, MacEachern JA. Hyperpycnal rivers and prodeltaic shelves in the Cretaceous seaway of North America. *Journal of Sedimentary Research* 2009, **79**(4)**:** 184-209.

4. Traykovski P, Geyer WR, Irish J, Lynch J. The role of wave-induced density-driven fluid mud flows for cross-shelf transport on the Eel River continental shelf. *Continental Shelf Research* 2000, **20**(16)**:** 2113-2140.

5. Barker SP, Haughton PD, McCaffrey WD, Archer SG, Hakes B. Development of rheological heterogeneity in clay-rich high-density turbidity currents: Aptian Britannia Sandstone Member, UK continental shelf. *Journal of Sedimentary Research* 2008, **78**(2)**:** 45-68.

6. McCave I, Jones K. Deposition of ungraded muds from high-density non-turbulent turbidity currents. *Nature* 1988, **333**(6170)**:** 250-252.

7. Haughton P, Davis C, McCaffrey W, Barker S. Hybrid sediment gravity flow deposits–classification, origin and significance. *Marine and Petroleum Geology* 2009, **26**(10)**:** 1900-1918.

8. Van Olphen H. *Introduction to Clay Colloid Chemistry*. Wiley, 1977.

9. Mehta AJ. *An Introduction to Hydraulics of Fine Sediment Transport*, vol. 38. World Scientific Publishing Co Inc, 2013.

10. Baas JH, Best JL. Turbulence modulation in clay-rich sediment-laden flows and some implications for sediment deposition. *Journal of Sedimentary Research* 2002, **72**(3)**:** 336-340.

11. Baas JH, Best JL, Peakall J, Wang M. A phase diagram for turbulent, transitional, and laminar clay suspension flows. *Journal of Sedimentary Research* 2009, **79**(4)**:** 162-183.

12. Leppard GG, Droppo IG. Overview of flocculation processes in freshwater ecosystems. *Flocculation in Natural and Engineered Environmental Systems*. CRC Press, 2004, pp 25-46.

13. Schindler RJ, Parsons DR, Ye L, Hope JA, Baas JH, Peakall J*, et al.* Sticky stuff: Redefining bedform prediction in modern and ancient environments. *Geology* 2015, **43**(5)**:** 399-402.

14. Tan X, Hu L, Reed AH, Furukawa Y, Zhang G. Flocculation and particle size analysis of expansive clay sediments affected by biological, chemical, and hydrodynamic factors. *Ocean Dynamics* 2014, **64**(1)**:** 143-157.

15. Vignaga E, Sloan DM, Luo X, Haynes H, Phoenix VR, Sloan WT. Erosion of biofilm-bound fluvial sediments. *Nature Geoscience* 2013, **6**(9)**:** 770-774.

16. Parsons DR, Schindler RJ, Hope JA, Malarkey J, Baas JH, Peakall J*, et al.* The role of biophysical cohesion on subaqueous bed form size. *Geophysical Research Letters* 2016.

17. Malarkey J, Baas JH, Hope JA, Aspden RJ, Parsons DR, Peakall J*, et al.* The pervasive role of biological cohesion in bedform development. *Nature Communications* 2015, **6**.

18. Tolhurst T, Gust G, Paterson D. The influence of an extracellular polymeric substance (EPS) on cohesive sediment stability. *Proceedings in Marine Science* 2002, **5:** 409-425.

19. DuBois M, Gilles KA, Hamilton JK, Rebers Pt, Smith F. Colorimetric method for determination of sugars and related substances. *Analytical chemistry* 1956, **28**(3)**:** 350-356.

20. Lowe DR. Sediment gravity flows: II Depositional models with special reference to the deposits of high-density turbidity currents. *Journal of Sedimentary Research* 1982, **52**(1)**:** 279-297.

21. Kneller B, Buckee C. The structure and fluid mechanics of turbidity currents: a review of some recent studies and their geological implications. *Sedimentology* 2000, **47:** 62-94.

22. Baker ML, Baas JH, Malarkey J, Jacinto RS, Craig MJ, Kane IA*, et al.* The effect of clay type on the properties of cohesive sediment gravity flows and their deposits. *Journal of Sedimentary Research*, in press.

23. Mulder T, Alexander J. The physical character of subaqueous sedimentary density flows and their deposits. *Sedimentology* 2001, **48**(2)**:** 269-299.

24. Middleton GV, Hampton MA. Sediment gravity flows: mechanics of flow and deposition *in* Turbidites and Deep-Water Sedimentation. *SEPM, Pacific Section, Short Course Lecture Notes* 1973**:** 1-38.

25. Wooldridge L, Worden R, Griffiths J, Thompson A, Chung P. Biofilm origin of clay-coated sand grains. *Geology* 2017, **45**(10)**:** 875-878.

26. Marr JG, Harff PA, Shanmugam G, Parker G. Experiments on subaqueous sandy gravity flows: the role of clay and water content in flow dynamics and depositional structures. *Geological Society of America Bulletin* 2001, **113**(11)**:** 1377-1386.

27. Iverson RM. The Physics of Debris Flows. *Reviews of Geophysics* 1997, **35**(3)**:** 245-296.

28. Talling PJ. Hybrid submarine flows comprising turbidity current and cohesive debris flow: Deposits, theoretical and experimental analyses, and generalized models. *Geosphere* 2013, **9**(3)**:** 460-488.

29. O'Brien JS, Julien PY. Laboratory analysis of mudflow properties. *Journal of Hydraulic Engineering* 1988, **114**(8)**:** 877-887.

30. Baas JH, Best JL, Peakall J. Depositional processes, bedform development and hybrid bed formation in rapidly decelerated cohesive (mud–sand) sediment flows. *Sedimentology* 2011, **58**(7)**:** 1953-1987.

31. Lowe DR, Guy M. Slurry-flow deposits in the Britannia Formation (Lower Cretaceous), North Sea: a new perspective on the turbidity current and debris flow problem. *Sedimentology* 2000, **47**(1)**:** 31-70.

32. Talling PJ, Masson DG, Sumner EJ, Malgesini G. Subaqueous sediment density flows: Depositional processes and deposit types. *Sedimentology* 2012, **59**(7)**:** 1937-2003.

33. Biscara L, Mulder T, Martinez P, Baudin F, Etcheber H, Jouanneau J-M*, et al.* Transport of terrestrial organic matter in the Ogooué deep sea turbidite system (Gabon). *Marine and Petroleum Geology* 2011, **28**(5)**:** 1061-1072.

34. Weimer P, Link MH. Global petroleum occurrences in submarine fans and turbidite systems. *Seismic Facies and Sedimentary Processes of Submarine Fans and Turbidite Systems*. Springer, 1991, pp 9-67.

35. Galy V, France-Lanord C, Beyssac O, Faure P, Kudrass H, Palhol F. Efficient organic carbon burial in the Bengal fan sustained by the Himalayan erosional system. *Nature* 2007, **450**(7168)**:** 407.

36. Berner RA. Atmospheric Carbon Dioxide Levels Over Phanerozoic time. *Science* 1990, **249:** 1382-1386.

37. Burdige DJ. Preservation of organic matter in marine sediments: controls, mechanisms, and an imbalance in sediment organic carbon budgets? *Chemical reviews* 2007, **107**(2)**:** 467-485.

38. de Haas H, van Weering TC, de Stigter H. Organic carbon in shelf seas: sinks or sources, processes and products. *Continental Shelf Research* 2002, **22**(5)**:** 691-717.

39. Muller-Karger FE, Varela R, Thunell R, Luerssen R, Hu C, Walsh JJ. The importance of continental margins in the global carbon cycle. *Geophysical Research Letters* 2005, **32**(1).

40. Premuzic ET, Benkovitz CM, Gaffney JS, Walsh JJ. The nature and distribution of organic matter in the surface sediments of world oceans and seas. *Organic Geochemistry* 1982, **4**(2)**:** 63-77.

41. Arthur M, Dean W, Stow D. Models for the deposition of Mesozoic-Cenozoic fine-grained organic-carbon-rich sediment in the deep sea. *Geological Society, London, Special Publications* 1984, **15**(1)**:** 527-560.

42. Bhaskar P, Bhosle NB. Microbial extracellular polymeric substances in marine biogeochemical processes. *Current Science* 2005, **88**(1)**:** 45-53.

43. Manning A, Friend P, Prowse N, Amos C. Estuarine mud flocculation properties determined using an annular mini-flume and the LabSFLOC system. *Continental Shelf Research* 2007, **27**(8)**:** 1080-1095.

44. Mietta F, Chassagne C, Manning AJ, Winterwerp JC. Influence of shear rate, organic matter content, pH and salinity on mud flocculation. *Ocean Dynamics* 2009, **59**(5)**:** 751-763.

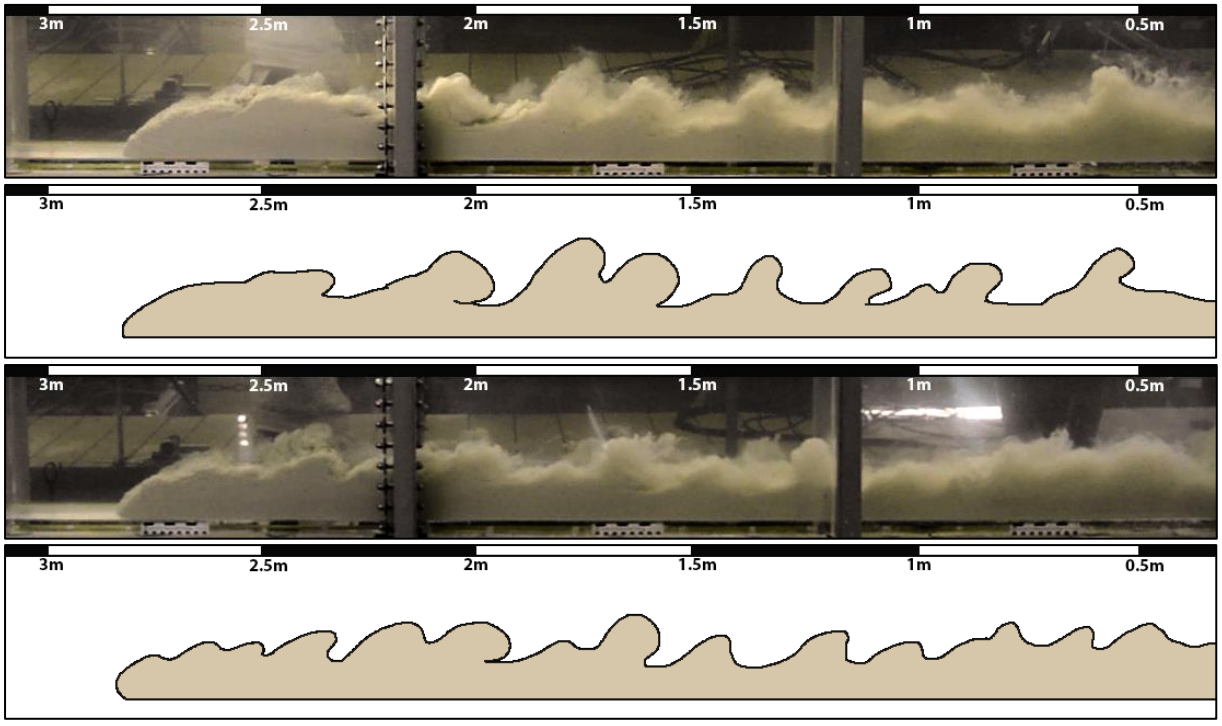

Figure 1 *Photograph and schematic drawing of low-density turbidity currents F01 (top) and F03 (bottom). Distance scale is from the lock-exchange gate. Flow direction is from right to left.*

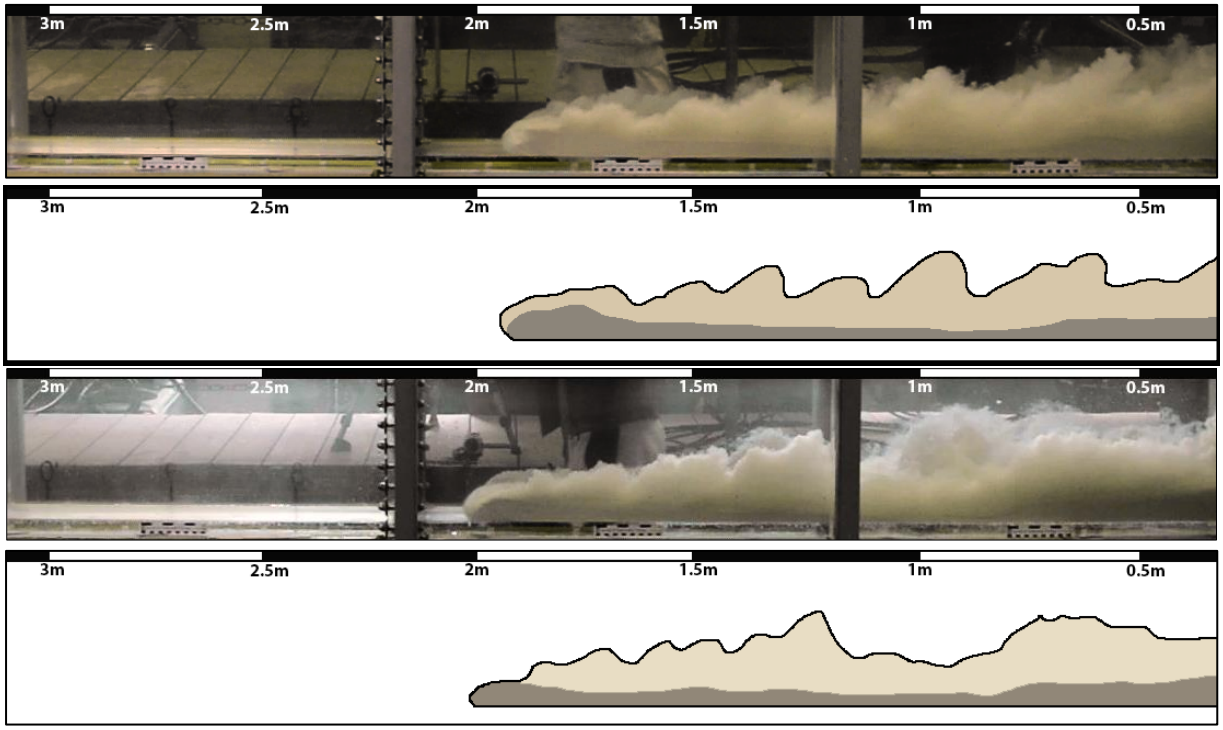

Figure 2 *Photograph and schematic drawing of high-density turbidity currents F16 (top) and F17 (bottom). Distance scale is from the lock-exchange gate. Flow direction is from right to left.*

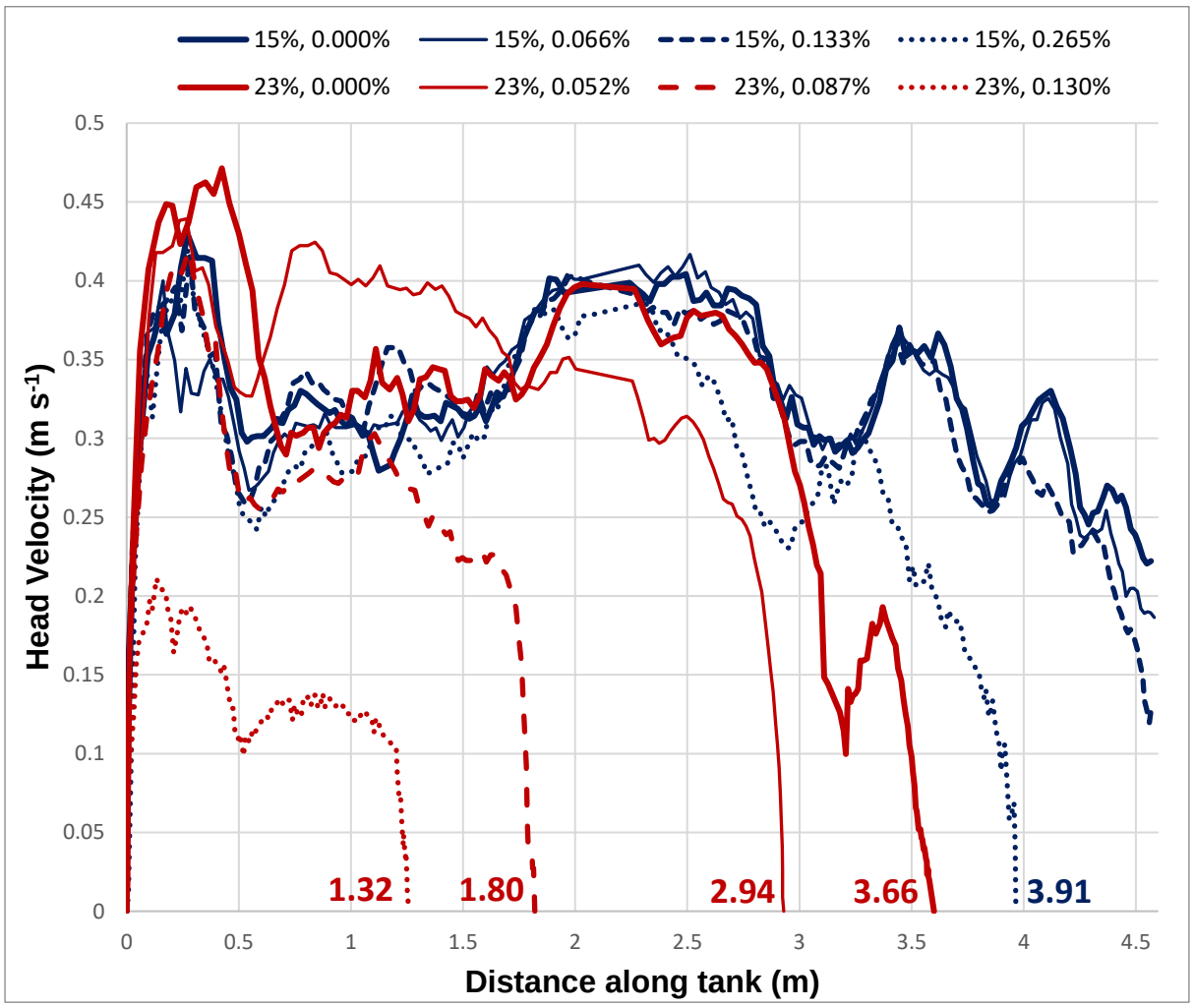

Figure 3 *Head velocity of 15% kaolinite (in dark blue) and 23% kaolinite (in red) with and without EPS against distance travelled along the tank. Numbers above the abscissa indicate run-out distances of flows that stopped before reaching the end of the tank.*

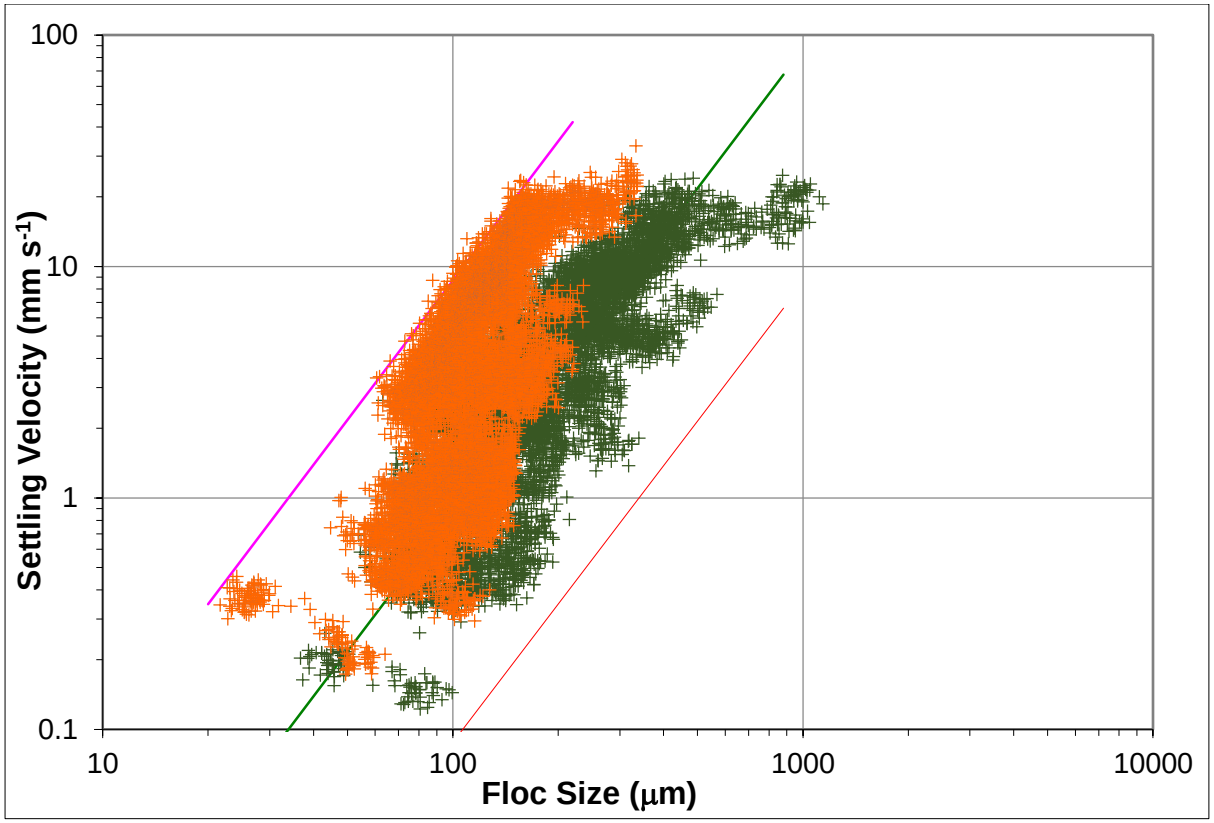

441

442 ***Figure 4*** *Distribution of floc size and settling velocity in samples extracted from the head of the EPS-*
443 *free 23% kaolinite flow (in orange) and the 23% flow that carried 0.052% EPS (in green). Both samples*
444 *were collected 12 mm above the base of the tank and at 60% of the respective run-out distance of each*
445 *flow. Diagonal lines represent contours of constant Stokes-equivalent excess density: 1600 kg* m^{-3} *(in*
446 *pink), 160 kg* m^{-3} *(in green) and 16 kg* m^{-3} *(in red).*

447

448

449 ***Table 1*** *Basic experimental data. Flow classifications follow the schemes of Lowe (1982), Kneller and*
450 *Buckee (2000), Mulder and Alexander (2001), Baas et al. (2009) and Baker et al. (in press).*
451 *ROD = run-out distance; $U_{h,max}$ = maximum head velocity, LDTC = low-density turbidity current;*
452 *HDTC = high-density turbidity current.*

Flow	Kaolinite C_{vol} (%)	EPS weight (%)	ROD (m)	$U_{h,max}$ (m s^{-1})	Flow Classification
F01	5	0	-	0.377	LDTC
F02	5	0.134	-	0.379	LDTC
F03	5	0.268	-	0.381	LDTC
F04	10	0	-	0.367	LDTC
F05	10	0.132	-	0.353	LDTC
F06	10	0.264	-	0.348	LDTC
F07	15	0	-	0.430	LDTC
F08	15	0.066	-	0.417	LDTC
F09	15	0.133	-	0.416	LDTC
F10	15	0.265	3.91	0.420	LDTC
F11	22	0	4.69	0.552	HDTC
F12	22	0.067	3.63	0.455	HDTC
F13	22	0.089	3.2	0.438	HDTC
F14	22	0.133	2.13	0.217	Cohesive Mudflow
F15	22	0.265	0.92	0.194	Cohesive Mudflow
F16	23	0	3.66	0.471	HDTC
F17	23	0.052	2.94	0.439	HDTC
F18	23	0.087	1.8	0.419	Cohesive Mudflow
F19	23	0.130	1.32	0.211	Cohesive Mudflow
F20	23	0.259	0.6	0.160	Slide

453

Supplementary Information

Methodology

Flume experiments. In order to determine the effect of biological cohesion on physically-cohesive sediment gravity flows, 20 laboratory experiments were conducted in a 5.0 m long, 0.2 m wide and 0.5 m deep smooth-bottomed lock-exchanged tank (Figure 1). A 0.31 m long reservoir at the upstream end of the tank was filled with a mixture of kaolinite clay (D_{50} = 9.1 µm), EPS, and seawater to a depth of 0.35 m. The remainder of the tank contained seawater to the same depth. All seawater was sourced from the Menai Strait (North Wales, United Kingdom). Xanthan gum, a commercially available anionic hydrophilic biopolymer, was used as a proxy for natural EPS. The two compartments of the tank were separated by a lock gate, which was lifted to generate the gravity flow.

To account for any time-dependent behaviour of the mixture, each suspension was prepared using the same method. First, the xanthan gum and kaolinite clay were mixed dry in a concrete mixer for 10 min to evenly disperse the EPS within the clay. The seawater was then added to and mixed with the dry material for 10 min in the concrete mixer. Next, the wet mixture was decanted into a container and mixed again for 3 min using a handheld concrete mixer to break up any remaining clumps of sediment, before leaving it to rest for 60 min. At the end of the resting time, the suspension was mixed a third time for 3 min and then added to the reservoir of the lock-exchange tank. Here, it was mixed for a final 30 seconds; immediately thereafter the lock gate was lifted as quickly as possible to generate the sediment gravity flow.

A high-definition video camera tracked the head of the flow as it progressed along the tank. The velocity of the head of the flow was calculated using the time-stamped video frames and a reference scale along the bottom of the tank.

LabSFLOC-2 methodology. Floc properties were measured using the LabSFLOC-2 (Laboratory Spectral Flocculation Characteristics) method. This method has been used successfully in numerous laboratory- and field-based flocculation studies and has demonstrated minimal floc disruption during acquisition[43, 44]. LabSFLOC-2 uses a non-intrusive Puffin Paescon UTC 341 high-resolution video camera positioned 75 mm above the base of a square settling column (190x10x10 mm). This camera observes particles settling in the centre of the column, using a depth of view of 1 mm at 45 mm in front of the lens. For the present experiments, the settling column was filled with seawater from the Menai Strait. To minimize density contrasts, care was taken to match the temperature with that of the seawater in the lock-exchange tank. A 0.4 m long glass pipette (4 mm internal diameter) was positioned in the lock-exchange tank at 60% of the anticipated flow run-out distance (based on an average of 12 replicate experiments). The end of the pipette was placed at 12 mm above the base of the tank, at the approximate height of the velocity maximum, informed by ultrasonic Doppler velocity profiler (UDVP) data. A small volume of mixed water, clay and EPS was then extracted from the passing head of the flow and immediately transferred to the LabSFLOC-2 settling column to minimise particle settling within the pipette. The sample was released from the pipette with the aperture of the pipette in contact with the water surface in the settling column through gravitational settling.

Supplementary Figures

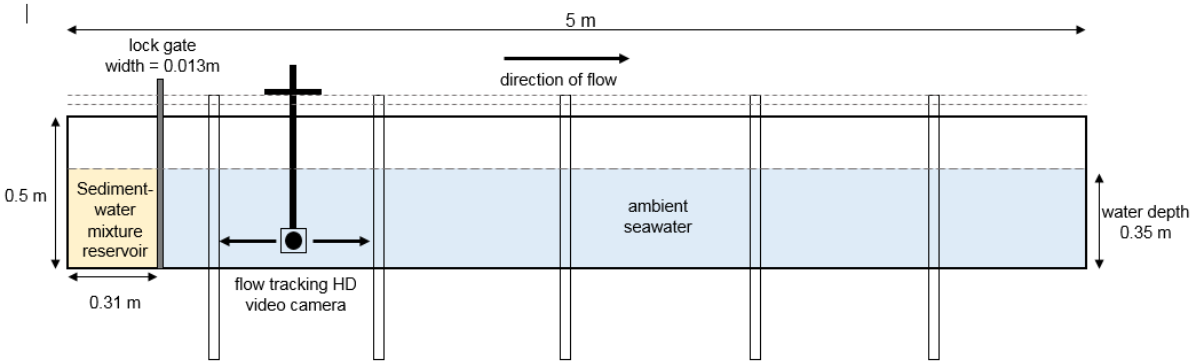

Supplementary Figure 1 *Schematic drawing of the lock-exchange tank.*

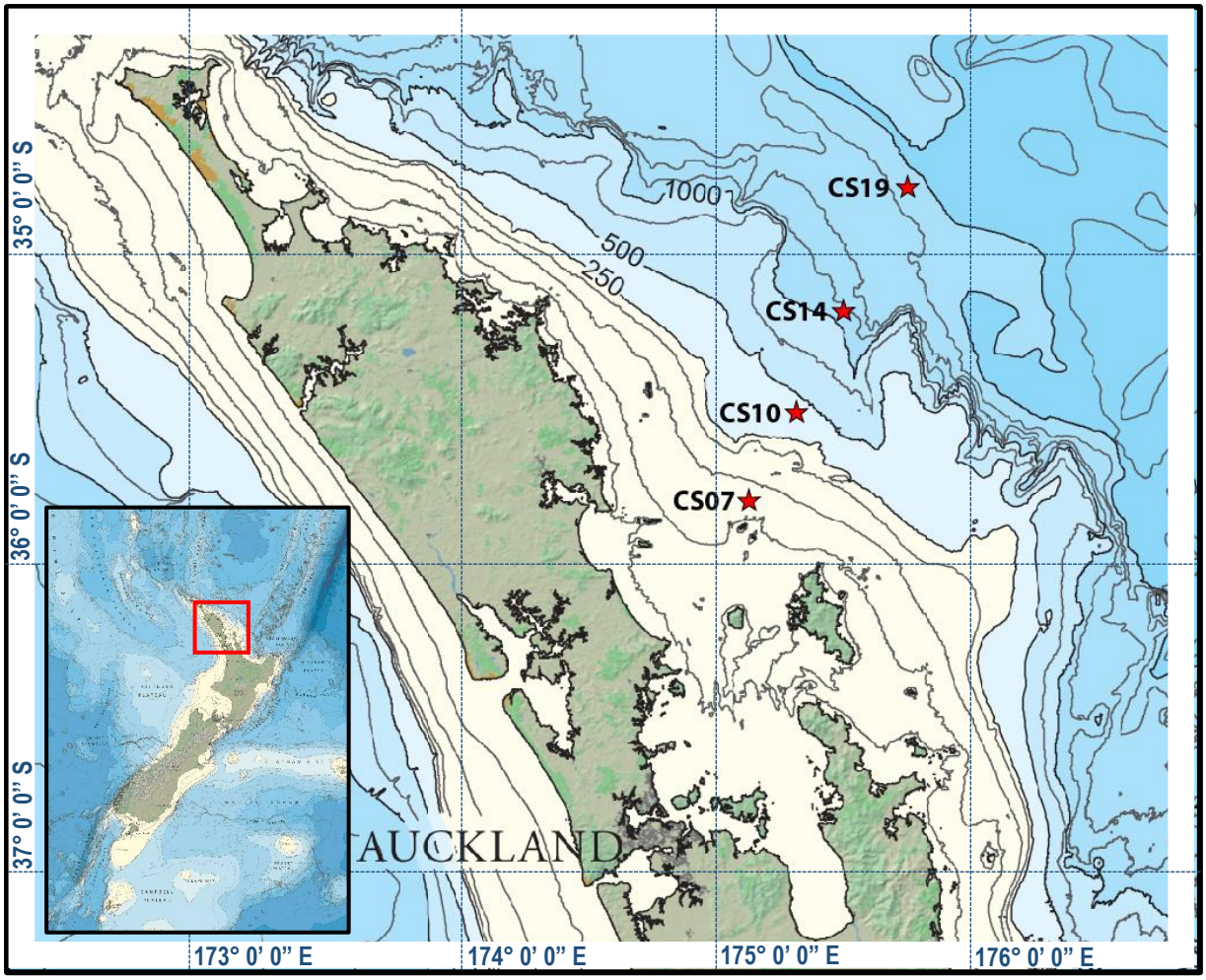

Supplementary Figure 2 *Outer Hauraki Gulf, New Zealand (see inset) with locations of cores CS07 (127 m water depth), CS10 (432 m), CS14 (1149 m) and CS19 (1872 m). Samples were collected with an Ocean Instruments MC-800 multi-corer (10 cm diameter cores).*

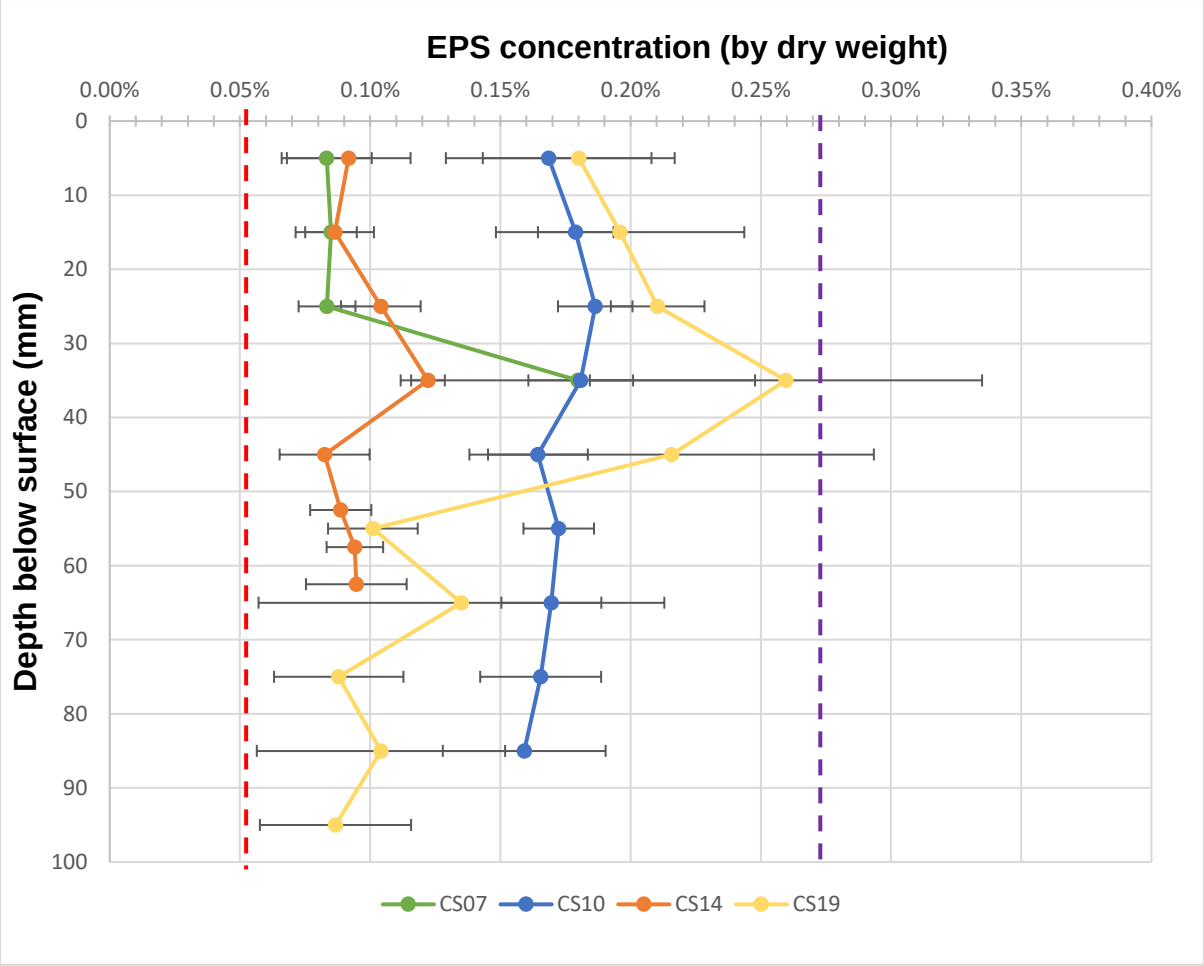

Supplementary Figure 3 *Vertical profiles of EPS taken from the outer Hauraki Gulf cores offshore New Zealand. The vertical lines represent dry weight quantities of EPS used within the experimental flows: (i) in red, 0.052% EPS in the bed reduced the run-out distance of a 23% kaolinite flow from 3.66 m (EPS-free equivalent) to 2.94 m; (ii) in purple, 0.259% EPS in the bed was the maximum amount of EPS used to simulate the 23% kaolinite flows, attaining a reduced run-out distance of 0.6 m. Horizontal lines denote standard deviation of the mean. Error bars correspond to the standard deviations (%) recorded for each EPS concentration (Supplementary Table 1).*

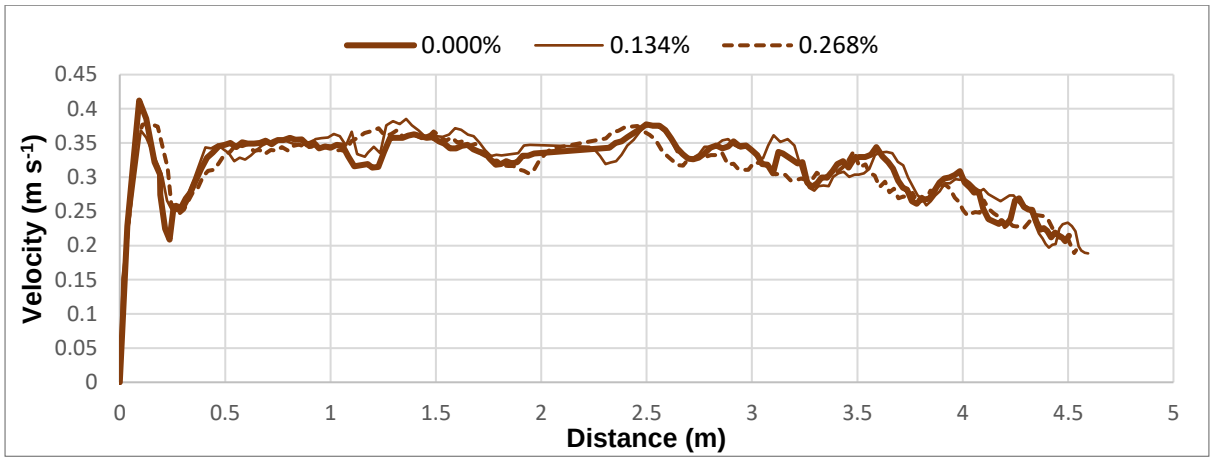

Supplementary Figure 4: *Head velocity of 5% kaolinite flows with and without EPS against distance travelled along the tank.*

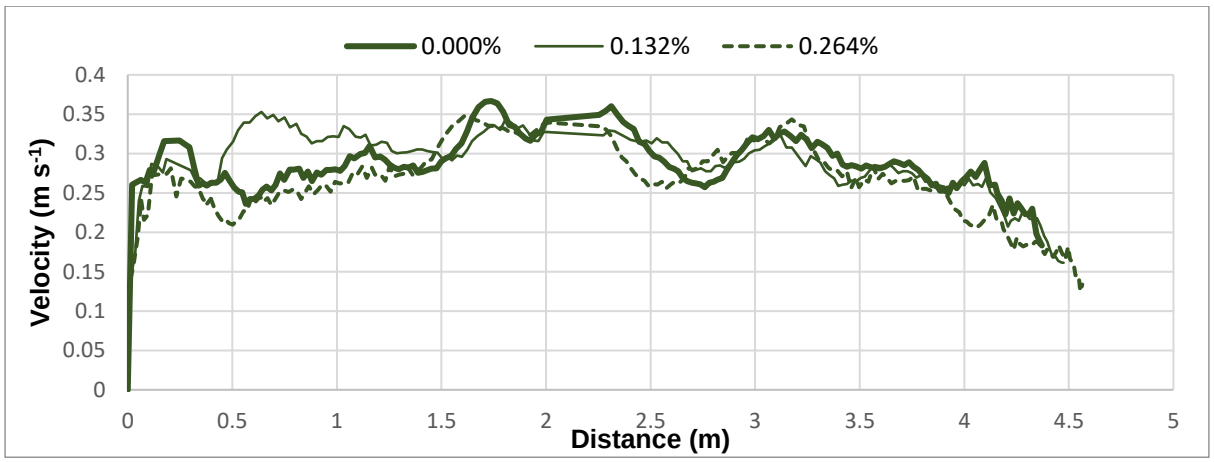

Supplementary Figure 5: *Head velocity of 10% kaolinite flows with and without EPS against distance travelled along the tank.*

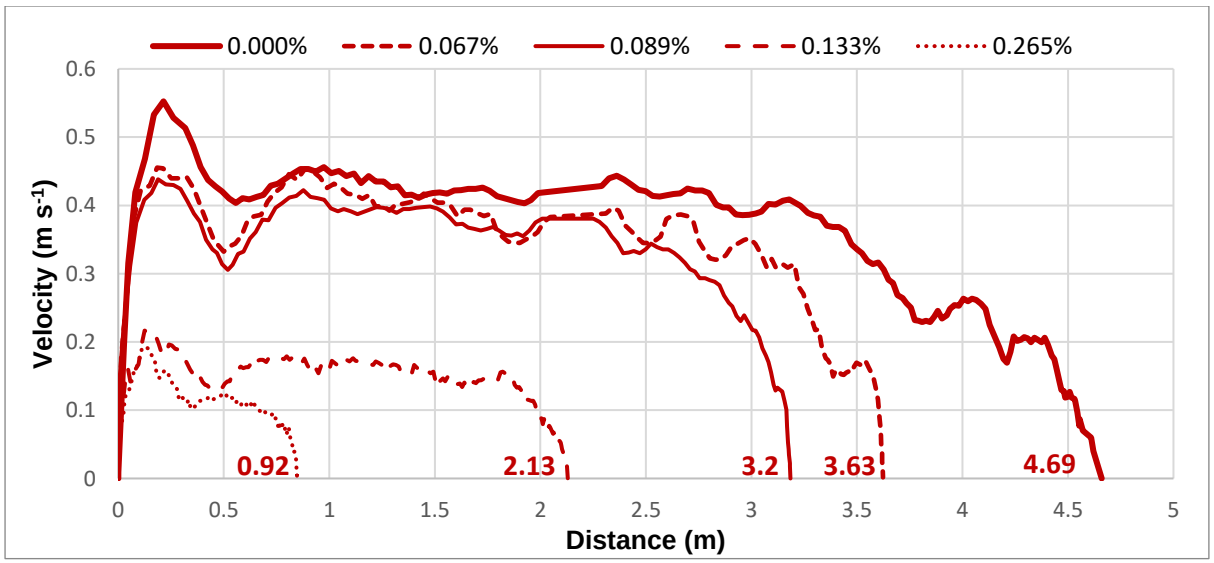

Supplementary Figure 6: *Head velocity of 22% kaolinite flows with and without EPS against distance travelled along the tank. Numbers above the abscissa indicate run-out distances of flows that stopped before reaching the end of the tank.*

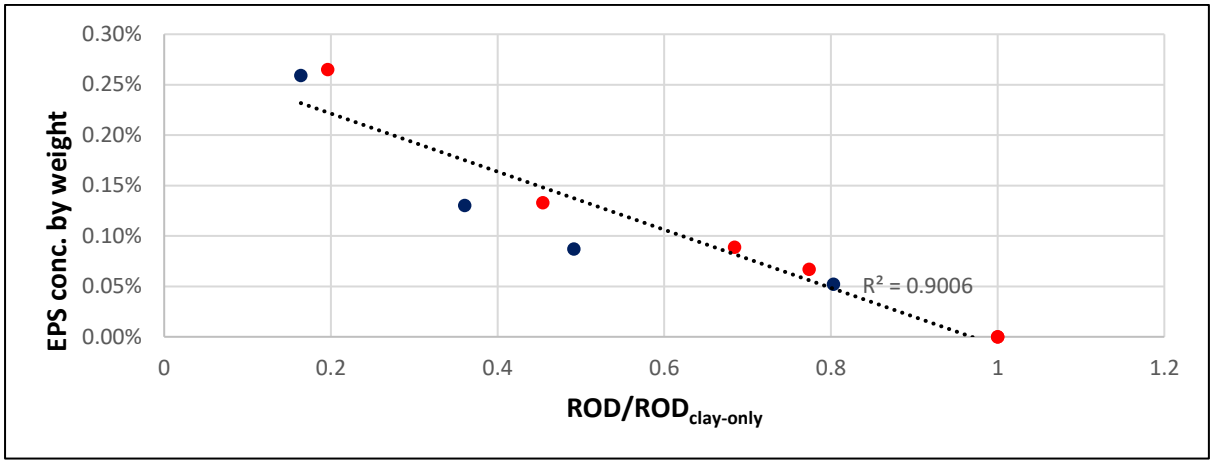

Supplementary Figure 7: *Normalized run-out distances (RODs) of 22% (in red) and 23% (in blue) kaolinite flows with and without EPS against the EPS concentration by weight added to the flow. Run-out distances were normalized to their respective clay-only run-out distance.*

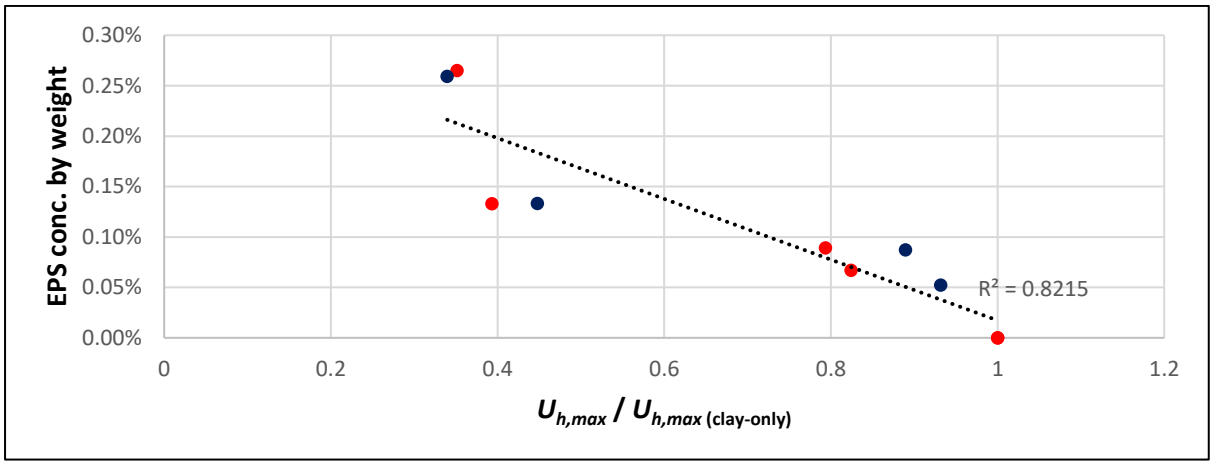

Supplementary Figure 8: *Normalized $U_{h,max}$ of 22% (in red) and 23% (in blue) kaolinite flows with and without EPS against the EPS concentration by weight added to the flow. $U_{h,max}$ values were normalized to their respective clay-only $U_{h,max}$* values.

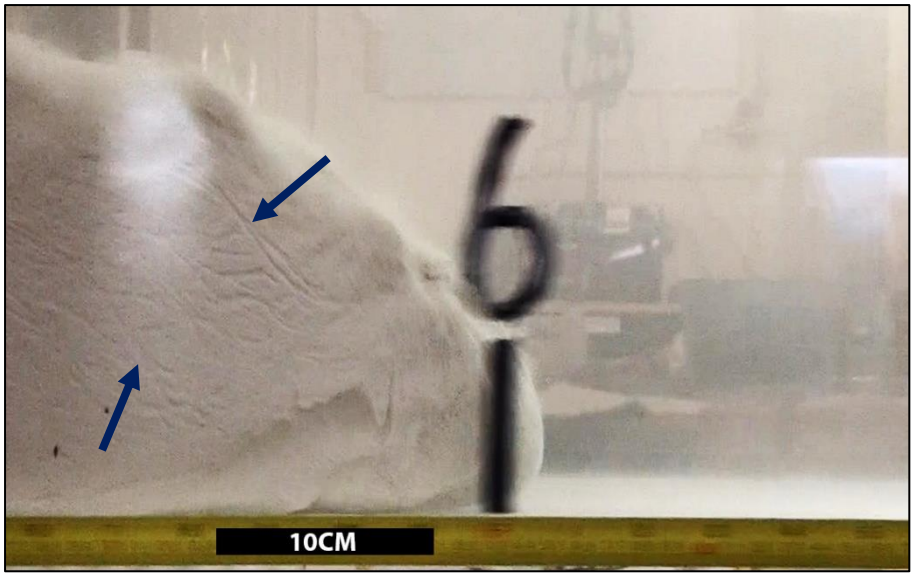

Supplementary Figure 9: *Head of 22% clay flow without EPS at 1.8 m downstream of flow release. Run-out distance = 4.69 m. Note pronounced coherent fluid entrainment structures indicated by the dark blue arrows. Flow direction is from left to right. Scale bar is 10 cm.*

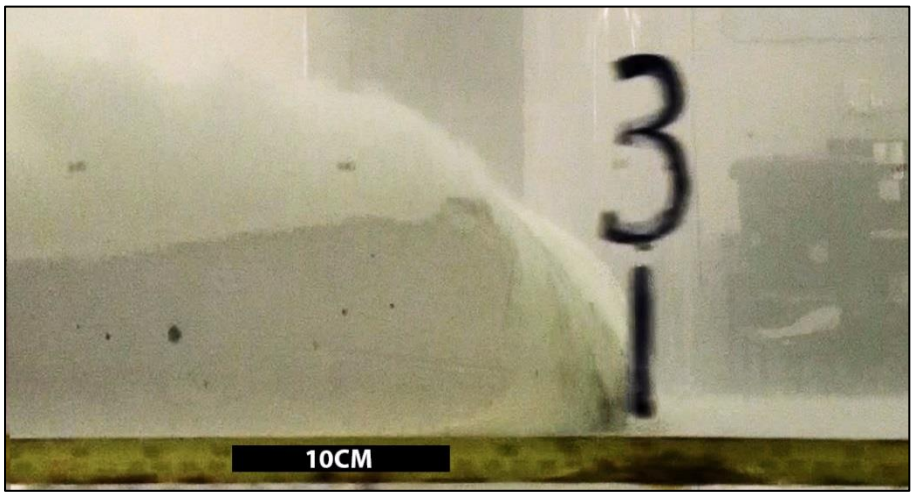

Supplementary Figure 10: *Head of 22% clay with 0.133% EPS at 0.9 m downstream of flow release. Run-out distance = 2.13 m. Note absence of coherent fluid entrainment structures. Flow direction is from left to right. Scale bar is 10 cm.*

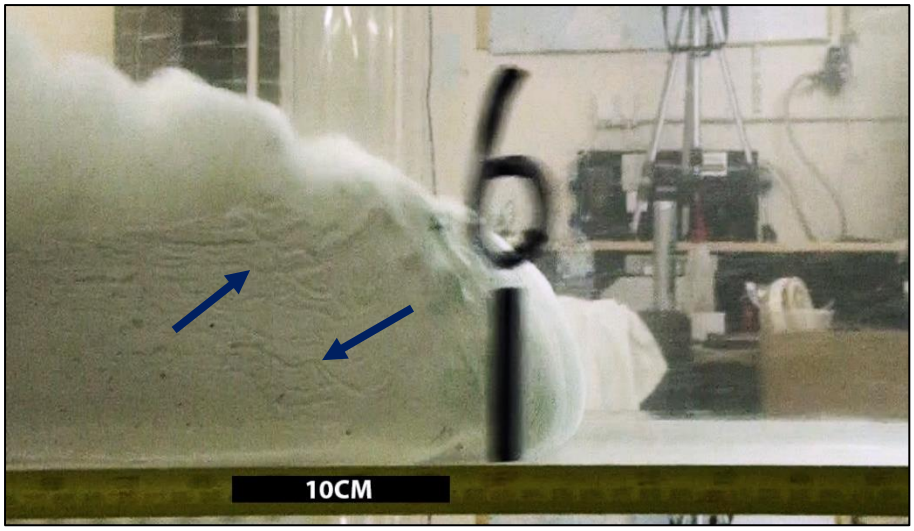

Supplementary Figure 11: *Head of 23% clay flow without EPS at 1.8 m downstream of flow release. Run-out distance = 3.66 m. Note presence of coherent fluid entrainment structures indicated by the dark blue arrows. Flow direction is from left to right. Scale bar is 10 cm.*

546 ***Supplementary Table 1*** *Summary of EPS data from cores collected during RV Tangaroa cruise*
547 *TAN1604 in the outer Hauraki Gulf, New Zealand.*

Core	*Depth (mm)*	*Total Carbohydrate, mean (%)*	*Total Carbohydrate, standard deviation (%)*	*D_{50} (µm)*	*Textural Description*
CS07	0-10	0.0833	0.0173	125.6	Slightly Gravelly Muddy Sand
CS07	10-20	0.0850	0.0099	97.42	Muddy Sand
CS07	20-30	0.0834	0.0109	69.52	Muddy Sand
CS07	30-40	0.1798	0.0680	49.23	Sandy Mud
CS10	0-10	0.1685	0.0395	74.75	Muddy Sand
CS10	10-20	0.1789	0.0145	88.49	Muddy Sand
CS10	20-30	0.1864	0.0143	93.73	Muddy Sand
CS10	30-40	0.1809	0.0201	93.73	Muddy Sand
CS10	40-50	0.1644	0.0192	93.73	Muddy Sand
CS10	50-60	0.1724	0.0136	81.16	Muddy Sand
CS10	60-70	0.1696	0.0192	81.61	Muddy Sand
CS10	70-80	0.1655	0.0232	82.68	Muddy Sand
CS10	80-90	0.1592	0.0313	77.13	Muddy Sand
CS14	0-10	0.0918	0.0237	64.69	Muddy Sand
CS14	10-20	0.0864	0.0150	63.01	Muddy Sand
CS14	20-30	0.1041	0.0153	81.13	Muddy Sand
CS14	30-40	0.1222	0.0065	81.13	Muddy Sand
CS14	40-50	0.0825	0.0173	81.13	Muddy Sand
CS14	50-55	0.0887	0.0117	83.05	Muddy Sand
CS14	55-60	0.0941	0.0109	83.05	Muddy Sand
CS14	60-65	0.0947	0.0193	71.57	Muddy Sand
CS19	0-10	0.1801	0.0368	15.00	Mud
CS19	10-20	0.1960	0.0477	15.44	Sandy Mud
CS19	20-30	0.2104	0.0180	14.88	Mud
CS19	30-40	0.2597	0.0753	14.42	Mud
CS19	40-50	0.2158	0.0777	14.33	Mud
CS19	50-60	0.1010	0.0172	15.53	Sandy Mud
CS19	60-70	0.1350	0.0779	20.16	Sandy Mud
CS19	70-80	0.0879	0.0248	18.47	Sandy Mud
CS19	80-90	0.1041	0.0477	17.16	Sandy Mud
CS19	90-100	0.0867	0.0290	16.28	Sandy Mud

548

549